

# $R$ -matrix type parametrization of the Jost function for extracting the resonance parameters from scattering data

P. Vaandrager<sup>a</sup>, M.L. Lekala<sup>a</sup> and S.A. Rakityansky<sup>b,c</sup>

<sup>a</sup> Department of Physics, University of South Africa (UNISA), South Africa

<sup>b</sup> Department of Physics, University of Pretoria, South Africa

<sup>c</sup> Lab of Theoretical Physics, JINR, Dubna, Russia

April 16, 2025

## Abstract

A new method is proposed for fitting non-relativistic binary-scattering data and for extracting the parameters of possible quantum resonances in the compound system that is formed during the collision. The method combines the well-known  $R$ -matrix approach with the analysis based on the semi-analytic representation of the Jost functions. It is shown that such a combination has the advantages of both these approaches, namely, the number of the fitting parameters remains relatively small (as for the  $R$ -matrix approach) and the proper analytic structure of the  $S$ -matrix is preserved (as for the Jost function method). It is also shown that the new formalism, although closely related to the  $R$ -matrix method, has the benefit of no dependence on an arbitrary channel radius. The efficiency and accuracy of the proposed method are tested using a model single-channel potential. Artificial “experimental” data generated with this potential are fitted, and its known resonances are successfully recovered as zeros of the Jost function on the appropriate sheet of the Riemann surface of the energy.

## 1 Introduction

In physics the resonance phenomena are associated with oscillations and waves. Since the motion of quantum objects is described by waves, it is not surprising that resonant states are ubiquitous in atomic and nuclear processes. In the collisions of such microscopic objects these resonances usually manifest themselves as certain irregularities in the energy dependence of the scattering cross-section [1]. In some rare cases the cross-section has a bell-shape maximum around the resonant collision energy,  $E_r$ . The width,  $\Gamma$ , of this bell at its half-height determines the half-life of the resonant state,  $T_{1/2} = \hbar \ln 2 / \Gamma$ . In most cases, however, the resonance irregularities are more complicated and it is not possible to directly deduce  $E_r$  and  $\Gamma$  from the measured cross-sections.

There are many different approaches to the problem of extracting these resonance parameters from the data [1, 2]. Most of them are based on the fact that each resonance corresponds to a pole of the  $S$ -matrix at a complex energy (see, for example, Ref. [3])

$$E = E_r - \frac{i}{2}\Gamma . \quad (1)$$

The common attribute for the majority of different approaches is that the data are fitted using the  $S$ -matrix, which can be parametrized in various ways. The poles of the  $S$ -matrix obtained from the fitting are then sought at complex energies. Not only do the differences among these approaches consist in the various ways of parametrizing the  $S$ -matrix, but also in the ways the  $S$ -matrix is continued to complex  $E$ .

The way in which such a continuation is performed plays an important role, because the  $S$ -matrix is a multivalued function of  $E$  and therefore it is defined on a complicated Riemann surface of this complex variable. This becomes especially important when the Coulomb forces are present, because in such a case the Riemann surface has a particularly complicated topology (see, for example, Ref. [4]). The parametrized  $S$ -matrix may be very good at real energies, but if a chosen functional form of this parametrization has inadequate analytic structure, the analytic continuation (especially near the branch point, i.e. near the threshold) can be inadequate as well.

A possible solution of this continuation-uncertainty problem was suggested in Ref. [5] (see also the book [4]), where semi-analytic expressions of the Jost functions,  $f_\ell^{(\text{in})}(E)$  and  $f_\ell^{(\text{out})}(E)$ , were rigorously derived for the case of charged particles. The  $S$ -matrix is just the ratio,

$$S(E) = f_\ell^{(\text{out})}(E) \left[ f_\ell^{(\text{in})}(E) \right]^{-1}, \quad (2)$$

of the outgoing and incoming Jost functions. In these expressions of the Jost functions, all the factors responsible for the multivaluedness and branching of the Riemann surface are given explicitly and in an exact way. It was shown that the remaining unknown factors are always single-valued and analytic functions of  $E$ . Any reasonable approximation of these factors does not affect proper analytic structure of the Jost functions. This fact allows one to reliably continue these functions (and thus the  $S$ -matrix) from the real energy axis to any relevant sheet of the Riemann surface (even if the branch-point is nearby). In particular, this is a reliable way of locating resonance poles of the  $S$ -matrix (2), when it is constructed from the fitting of experimental data.

In Ref. [5] it was suggested to approximate the single-valued factors of the Jost functions by polynomials of the variable  $(E - E_0)$ , with  $E_0$  on the real axis and with the coefficients of these polynomials being the free parameters that are used to fit experimental data. Such an approach was tested on a model problem [6] and then applied to analyse several nuclear reactions [7–10], where the resonances were located and the corresponding residues of the  $S$ -matrix and the Asymptotic Normalisation Coefficient (ANC) were determined. Although the method works and proved to be accurate, it has a significant drawback, namely, that the number of the fitting parameters is too large (typically a few dozen).

Such a large number is in a drastic contrast with the number of parameters usually required within the most famous and widely used  $R$ -matrix approach [11–14], where it is possible to nicely fit the data with the help of just several parameters. On the other hand, the  $R$ -matrix method is not without its own drawbacks. Firstly, everything in this method depends on the choice of a rather arbitrary channel radius, at which the inner and outer wave functions match. Secondly, the analytic structure of the  $S$ -matrix obtained from the  $R$ -matrix is obscure, which makes its analytic continuation obscure as well.

In the present work we combine the advantages of both the  $R$ -matrix and the Jost function theories, namely, a small number of the fitting parameters (a feature of the  $R$ -matrix) with proper analytic structure (a feature of the Jost function method). In order to present the basic idea clearly, as well as to demonstrate the accuracy and efficiency of the proposed method, we consider a single-channel problem with a model potential. Exactly calculated cross sections for this potential are used as artificial “experimental” data points, which are fitted using the modified Jost-function method. The new method is tested by recovering some of the known resonances for this potential.

In the next section, the original Jost-function fitting procedure for a single-channel problem is described. Then, in Section 3, the relationship between the Jost function and  $R$ -matrix methods is shown. Section 4 presents the proposed modification of the Jost function fitting procedure. In Section 6, a test potential is described. The results from performing the modified Jost-function fitting of the artificial data are then given, i.e. the fitting of the total cross-section generated by the test potential, for  $\ell_{\text{max}} \leq 2$ . The conclusion follows.

## 2 Single-channel Jost-function analysis

A comprehensive presentation of the Jost function theory can be found in the book, Ref. [4]. For the reader's convenience, we give a very concise description of the main equations from that book, which are relevant to using the Jost functions for the analysis of a set of single-channel scattering data.

The single-channel Jost functions are defined via the regular solution,  $\phi_\ell(E, r)$ , of the radial Schrödinger equation, which (by definition) behaves like the Riccati-Bessel function near the origin<sup>1</sup>,

$$\phi_\ell(E, r) \xrightarrow{r \rightarrow 0} j_\ell(kr) . \quad (3)$$

The Jost functions,  $f_\ell^{(\text{in})}(E)$  and  $f_\ell^{(\text{out})}(E)$ , are the amplitudes of the incoming and outgoing Coulomb-modified spherical waves,  $H_\ell^{(\mp)}(\eta, kr)$ , in the asymptotic behaviour of this solution,

$$\phi_\ell(E, r) \xrightarrow{r \rightarrow \infty} H_\ell^{(-)}(\eta, kr) e^{i\delta_\ell^c} f_\ell^{(\text{in})}(E) + H_\ell^{(+)}(\eta, kr) e^{-i\delta_\ell^c} f_\ell^{(\text{out})}(E) , \quad (4)$$

where

$$\begin{aligned} H_\ell^{(\pm)}(\eta, kr) &= F_\ell(\eta, kr) \mp iG_\ell(\eta, kr) \\ &\xrightarrow{r \rightarrow \infty} \mp i \exp \left\{ \pm i \left[ kr - \frac{\ell\pi}{2} - \eta \ln(2kr) + \delta_\ell^c \right] \right\} , \end{aligned} \quad (5)$$

with  $F_\ell$  and  $G_\ell$  being the standard regular and irregular Coulomb functions. The energy dependent quantity  $\delta_\ell^c$  is the pure Coulomb phase shift,

$$\delta_\ell^c(\eta) = \frac{1}{2i} \ln \frac{\Gamma(\ell + 1 + i\eta)}{\Gamma(\ell + 1 - i\eta)} . \quad (6)$$

This and the other functions in the above equations depend on the energy via the wave number,  $k$ , and the Sommerfeld parameter,  $\eta$ :

$$k^2 = \frac{2\mu E}{\hbar^2}, \quad \eta = \frac{\mu e^2 Z_1 Z_2}{k\hbar^2}, \quad (7)$$

where  $\mu$  is the reduced mass while  $Z_1$  and  $Z_2$  are the charges.

The Jost functions have the following structure (a detailed derivation can be found in Sec. 8.2.6 of the book [4]):

$$f_\ell^{(\text{in/out})}(E) = e^{\mp i\delta_\ell^c} k^\ell \left\{ \frac{k}{D_\ell(\eta, k)} A_\ell(E) - [M(k) \pm i] D_\ell(\eta, k) B_\ell(E) \right\}, \quad (8)$$

where

$$D_\ell(\eta, k) = C_\ell(\eta) k^{\ell+1}, \quad M(k) = \frac{2\eta h(\eta)}{C_0^2(\eta)}, \quad (9)$$

$$\begin{aligned} h(\eta) &= \frac{1}{2} [\psi(1 + i\eta) + \psi(1 - i\eta)] - \ln \eta, \\ \psi(z) &= \frac{\Gamma'(z)}{\Gamma(z)}, \end{aligned} \quad (10)$$

and the Coulomb barrier factor,

$$C_\ell(\eta) = \frac{e^{-\pi\eta/2}}{\Gamma(\ell + 1)} \exp \left\{ \frac{1}{2} \left[ \ln \Gamma(\ell + 1 + i\eta) + \ln \Gamma(\ell + 1 - i\eta) \right] \right\}, \quad (11)$$

---

<sup>1</sup>It should be noted that this definition remains the same even if the Coulomb potential is present. This special regular solution is always defined in such a way: that near the origin, it behaves the same as for completely free motion. The effect of the Coulomb forces (if any) manifest in the behaviour of the regular solution at large distances. The function  $j_\ell(kr)$  in Eq. (3) cannot be replaced with  $F_\ell(\eta, kr)$  because otherwise, for a pure Coulomb problem, the Jost functions would be trivial, i.e. equal to one.

is defined in such a way that for neutral particles it becomes unity,  $C_\ell(0) = 1$ , for all  $\ell$ . This means that the barrier factor (11) is obtained from the one defined, for example, in Ref. [15], by multiplying with  $(2\ell + 1)!!$ .

It should be emphasized that the representation (8) is exact and valid for any single-channel, two-body system. For any chosen two-body potential, all the explicit factors remain the same in this representation. The potential only determines the unknown factors  $A_\ell(E)$  and  $B_\ell(E)$ . The important property of these unknown factors is that they are always single-valued, analytic functions of the variable  $E$ , and therefore are defined on a simple complex-energy plane without any branching points. All the troubles associated with the multivaluedness and branching of the Riemann surface are correctly taken into account by the explicitly given factors in (8). Any reasonable approximation of  $A_\ell(E)$  and  $B_\ell(E)$  does not affect the correct analytic structure of the Jost functions.

The  $S$ -matrix (2) in the single-channel case takes the form of a simple ratio,

$$S_\ell(E) = e^{2i\delta_\ell^c} \frac{kA_\ell(E) - [M(k) - i] D_\ell^2(\eta, k) B_\ell(E)}{kA_\ell(E) - [M(k) + i] D_\ell^2(\eta, k) B_\ell(E)}. \quad (12)$$

Experimental data-points that are fitted via this  $S$ -matrix, are either the phase-shifts or the scattering cross-sections at specific energies. The total scattering cross-section,

$$\sigma_{\text{total}}(E) = \sum_{\ell=0}^{\ell_{\text{max}}} \sigma_\ell(E), \quad (13)$$

is the sum of all the partial-wave cross-sections,

$$\sigma_\ell(E) = \frac{\pi}{k^2} (2\ell + 1) |S_\ell(E) - 1|^2, \quad (14)$$

up to some  $\ell_{\text{max}}$  that is deemed to make a noticeable contribution.

In the original method based on the semi-analytic representation (8), the functions  $A_\ell(E)$  and  $B_\ell(E)$  were approximated by several terms of the Taylor expansions around a point  $E_0$  on the real axis,

$$A_\ell(E) \approx \sum_{n=0}^N a_n(\ell, E_0) (E - E_0)^n, \quad B_\ell(E) \approx \sum_{n=0}^N b_n(\ell, E_0) (E - E_0)^n, \quad (15)$$

where the coefficients  $a_n$  and  $b_n$  served as the fitting parameters. The only drawback of this method is a large number of the parameters. In order to reduce this number, we propose a different approximation of  $A_\ell(E)$  and  $B_\ell(E)$ , which is inspired by the  $R$ -matrix theory. The Jost function method modified in this way is described further down in Sec. 4.

### 3 Relation between the $R$ -matrix and the Jost functions

The following expression of the single-channel Jost function in terms of the  $R$ -matrix was obtained in Ref. [16],

$$f_\ell^{(\text{in/out})}(E) = \frac{\pm i e^{\mp i\delta_\ell^c} k^\ell}{Q_\ell(E, B_R)} \left\{ H_\ell^{(\pm)}(\eta, ka) - \left[ a \frac{dH_\ell^{(\pm)}(\eta, kr)}{dr} \Big|_{r=a} - B_R H_\ell^{(\pm)}(\eta, ka) \right] R_\ell(E, B_R) \right\}, \quad (16)$$

where  $B_R$  is the so-called boundary parameter. Although this parameter is present in Eq. (16), it can be shown that the Jost function and therefore the  $S$ -matrix are actually independent

of  $B_R$  [12, 16]. This is why it is usually chosen as  $B_R = 0$  in the majority of analyses. The  $R$ -matrix has the following standard form [12, 14]:

$$R_\ell(E, B_R) = \sum_{n=1}^N \frac{[\gamma_{n\ell}(B_R)]^2}{E_{n\ell} - E}, \quad (17)$$

where the values  $\gamma_{n\ell}$  are either the fitting parameters (phenomenological  $R$ -matrix) or can be calculated with a given potential (computational  $R$ -matrix).

The parameter,  $a$ , is very important in the  $R$ -matrix theory. This is the distance at which the “inner” and the “outer” wave functions match, i.e. it is assumed that at  $r = a$ , the wave function converges to its asymptotic form. The choice of this parameter is rather arbitrary, which is one of the flaws of the  $R$ -matrix theory.

The real energies  $E_{n\ell}$  ( $n = 1, 2, \dots, N$ ) are the parameters that, in fact, make the  $R$ -matrix theory very efficient. It is with these parameters that one can introduce some prior (approximate) knowledge about the physical system into the analysis. From the outset, these energies are fixed to known bound states and to the real parts of known (or approximately known) resonance energies.

The function,  $Q_\ell(E, B_R)$ , is similar to the  $R$ -matrix [16]:

$$Q_\ell(E, B_R) = \sum_{n=1}^N \frac{\lambda_{n\ell}(B_R)\gamma_{n\ell}(B_R)}{E_{n\ell} - E}, \quad (18)$$

where  $\lambda_{n\ell}(B_R)$  are unknown, real quantities. The function,  $Q_\ell(E, B_R)$ , is not required in determining any measurable physical values. Indeed, this function is a common factor in (16) for both  $f_\ell^{(\text{in})}(E)$  and  $f_\ell^{(\text{out})}(E)$  and therefore it cancels out in the  $S$ -matrix (2):

$$S_\ell = -e^{2i\delta_\ell} \frac{H_\ell^{(-)} - [aH_\ell'^{(-)} - B_R H_\ell^{(-)}]R_\ell}{H_\ell^{(+)} - [aH_\ell'^{(+)} - B_R H_\ell^{(+)}]R_\ell}, \quad (19)$$

where, in order to simplify notation, we drop all the arguments of the functions and denote by a prime the derivative over  $r$ . In fact, the numerator and denominator in this equation are given by Eq. (16) and therefore it is easy to recover these arguments, when necessary.

We have two different representations of the Jost functions: first, by Eq. (8) in terms of  $A_\ell(E)$  and  $B_\ell(E)$ , and second, by Eq. (16) in terms of the  $R$ -matrix. Their equivalence can be shown if we choose the functions  $A_\ell(E)$  and  $B_\ell(E)$  in the following special forms:

$$A_\ell(E) = \frac{D_\ell(\eta, k)}{kQ_\ell(E, B_R)} \left\{ J_\ell(\eta, ka) - \left[ a \frac{dJ_\ell(\eta, kr)}{dr} \Big|_{r=a} - B_R J_\ell(\eta, ka) \right] R_\ell(E, B_R) \right\} \quad (20)$$

and

$$B_\ell(E) = \frac{[D_\ell(\eta, k)]^{-1}}{Q_\ell(E, B_R)} \left\{ F_\ell(\eta, ka) - \left[ a \frac{dF_\ell(\eta, kr)}{dr} \Big|_{r=a} - B_R F_\ell(\eta, ka) \right] R_\ell(E, B_R) \right\}, \quad (21)$$

where

$$J_\ell(\eta, kr) = G_\ell(\eta, kr) - M(\eta)F_\ell(\eta, kr). \quad (22)$$

As we know [4], the functions  $A_\ell(E)$  and  $B_\ell(E)$  in Eq. (8) are single-valued and analytic. However, when written in terms of the  $R$ -matrix as given above, their analyticity is not obvious. In order to check if Eqs. (20) and (21) give single-valued analytic functions, we transform them by replacing the Coulomb functions by their special representations that were derived by Humblet [17]. He showed that the regular and irregular Coulomb functions have the following structure (see also Refs. [4, 5]):

$$F_\ell(\eta, kr) = D_\ell(\eta, k)\tilde{F}_\ell(E, r), \quad (23)$$

$$G_\ell(\eta, kr) = M(\eta)D_\ell(\eta, k)\tilde{F}_\ell(E, r) + \frac{k}{D_\ell(\eta, k)}\tilde{G}_\ell(E, r), \quad (24)$$

where  $\tilde{F}_\ell(E, r)$  and  $\tilde{G}_\ell(E, r)$  are single-valued and analytic in  $E$ . Substituting these expressions in Eqs. (20) and (21), we obtain:

$$A_\ell(E) = \frac{\tilde{G}_\ell(E, a)}{Q_\ell(E, B_R)} - \left[ a \frac{d\tilde{G}_\ell(E, r)}{dr} \Big|_{r=a} - B_R \tilde{G}_\ell(E, a) \right] \frac{R_\ell(E, B_R)}{Q_\ell(E, B_R)} \quad (25)$$

and

$$B_\ell(E) = -\frac{\tilde{F}_\ell(E, a)}{Q_\ell(E, B_R)} + \left[ a \frac{d\tilde{F}_\ell(E, r)}{dr} \Big|_{r=a} - B_R \tilde{F}_\ell(E, a) \right] \frac{R_\ell(E, B_R)}{Q_\ell(E, B_R)}. \quad (26)$$

The dependence on the odd powers of  $k$  (which causes the square-root branching,  $k \sim \sqrt{E}$ ) as well as on  $M(\eta)$  (which causes the logarithmic branching) have cancelled out and therefore  $A_\ell(E)$  and  $B_\ell(E)$  are single-valued in variable  $E$ .

What about analyticity of  $A_\ell(E)$  and  $B_\ell(E)$  given by Eqs. (25, 26)? In order to answer this question, we re-write the representations (17, 18) as

$$R_\ell(E, B_R) = \frac{1}{\mathcal{P}_0(E)} \sum_{n=1}^N \gamma_{n\ell}^2 \mathcal{P}_n(E), \quad (27)$$

$$Q_\ell(E, B_R) = \frac{1}{\mathcal{P}_0(E)} \sum_{n=1}^N \lambda_{n\ell} \gamma_{n\ell} \mathcal{P}_n(E), \quad (28)$$

where  $\mathcal{P}_n(E)$  ( $n = 0, 1, 2, \dots, N$ ) are the following polynomials:

$$\mathcal{P}_0(E) = \prod_{n=1}^N (E_{n\ell} - E), \quad (29)$$

$$\mathcal{P}_n(E) = \frac{\mathcal{P}_0(E)}{E_{n\ell} - E}, \quad \text{for } n > 0. \quad (30)$$

It is clear that both  $R_\ell(E, B_R)$  and  $Q_\ell(E, B_R)$  are singular at all  $N$  points  $E = E_{n\ell}$ ,  $n = 1, 2, \dots, N$ . However, in their ratio,  $R_\ell/Q_\ell$ , the denominators  $\mathcal{P}_0(E)$  cancel out, which removes these singularities. The inverted  $1/Q_\ell(E, B_R)$  is non-singular (equals to zero) at these poles as well. Unfortunately, these facts are not sufficient to make  $R_\ell/Q_\ell$  and  $1/Q_\ell$  analytic. The numerator on the right-hand side of Eq. (28) is a polynomial of the order  $(N - 1)$  in variable  $E$  and thus has  $(N - 1)$  zeros in the complex  $E$ -plane. As a consequence, the right hand sides of Eqs. (25, 26) have first-order poles at these zeros.

Therefore the functions  $A_\ell(E)$  and  $B_\ell(E)$ , when obtained within the  $R$ -matrix theory, are single-valued (as it should be), but are not analytic on the whole  $E$ -plane. They are singular at  $(N - 1)$  isolated points, i.e. they are meromorphic. This fact illustrates our statement given in the Introduction, that the analytic structure of the  $R$ -matrix is obscure, which makes its analytic continuation to complex energies not completely reliable. This is where the Jost function (which is free of such defects) could be of help.

## 4 Modified Jost-function analysis

The semi-analytic representations of the Jost functions (8) are exact and valid for any potential. When fitting experimental data, we vary the functions  $A_\ell(E)$  and  $B_\ell(E)$ , which are the only unknown factors in these representations. In order to vary  $A_\ell(E)$  and  $B_\ell(E)$ , we can choose any appropriate parametrization, with the condition that they are single-valued and analytic on the whole complex  $E$ -plane.

Originally, it was suggested to use several terms of the Taylor series to parametrize these functions, as is given by Eq. (15). A Taylor series gives a good approximation of a function

near the central point of the expansion, i.e. around  $E = E_0$ , in our case. When  $E$  moves away from  $E_0$ , the accuracy drops. This is why, within such an approach, one has to use many Taylor terms. Even with a large number of terms, the energy range where the fitting is good, remains narrow.

In order to circumvent this difficulty, we can use the parametrization inspired by the  $R$ -matrix theory. This can be done in the following way. Looking at Eqs. (25, 26), we see that most of the factors are the same for any physical system, i.e. they are just some combination of the Coulomb-related functions and do not depend on the potential. The only factors determined by the potential, are the functions  $R_\ell$  and  $Q_\ell$  given by Eqs. (27, 28). Therefore  $A_\ell(E)$  and  $B_\ell(E)$  can be represented as linear combinations of the polynomials  $\mathcal{P}_n(E)$  ( $n = 0, 1, 2, \dots, N$ ). As was discussed in the preceding section, in these equations, a common denominator is present, which is a polynomial of the order  $(N - 1)$ . Since this polynomial makes  $A_\ell(E)$  and  $B_\ell(E)$  meromorphic instead of analytic and since it cancels out in the expression (12) for the  $S$ -matrix anyway, we can ignore it. Perhaps it should be emphasized that the choice of the parametrization of the functions  $A_\ell(E)$  and  $B_\ell(E)$  is rather arbitrary. We therefore have some freedom in this, and we do not violate or distort something by ignoring the common denominator.

Based on this simple reasoning, we replace the Taylor expansions (15) with the following:

$$A_\ell(E) = \sum_{n=0}^N \alpha_{n\ell} \mathcal{P}_n(E), \quad B_\ell(E) = \sum_{n=0}^N \beta_{n\ell} \mathcal{P}_n(E), \quad (31)$$

where the real numbers  $\alpha_{n\ell}$  and  $\beta_{n\ell}$  can be used as fitting parameters. In contrast to the Taylor series (15), the parameters in Eqs. (31) do not depend on the (arbitrarily chosen) central point  $E_0$ . This new parametrization incorporates the prior (approximate) knowledge of the resonance energies,  $E_{n\ell}$ , which should make the fitting of the data easier and more accurate.

## 5 Fitting procedure

In a typical scenario, a set of experimental total cross-section data points is available,

$$\sigma_{\text{total}}(E_i) \pm \Delta_i, \quad i = 1, 2, \dots, N^{(\text{data})} \quad (32)$$

with the corresponding experimental errors  $\Delta_i$ , measured at the collision energies  $E_i$ . In order to fit this set of data points, we parametrize the functions  $A_\ell(E)$  and  $B_\ell(E)$  as is given by Eqs. (31). We then substitute them in the  $S$ -matrix (12) and obtain the total cross-section (13) by summing over several partial cross-sections (14) from  $\ell = 0$  up to some  $\ell_{\text{max}}$ , that we consider as giving a noticeable contributions to the total cross-section. As a result of such a summation, for each data point we obtain the fitted cross-section  $\sigma_{\text{fit}}(E_i)$ , which depends on the factors  $\alpha_{n\ell}$  and  $\beta_{n\ell}$ , as well as the energies,  $E_{n\ell}$ , that are a part of the polynomials (29, 30).

The set of the energies  $E_{n\ell}$  is chosen in the same way as in the  $R$ -matrix analysis. In simple words, this is done as follows: Inspecting the experimental data, we find the collision energies around which  $\sigma_{\text{total}}(E)$  shows some irregularities, i.e. where it is noticeably different from a smooth monotone function. Such points are considered as “suspected resonances” and are included in the set of  $E_{n\ell}$ . It should be emphasized that in most cases, the final real parts of the resonance energies (1) differ from the chosen  $E_{n\ell}$ . This means that any small shifts (either to the left or to the right) of  $E_{n\ell}$  can only change the optimal values of  $\alpha_{n\ell}$  and  $\beta_{n\ell}$ , but do not affect the final results. However, the closer a chosen  $E_{n\ell}$  is to the actual  $E_r$ , the better the fit. In a sense, the choice of these energy points, based on the inspection of the data, is a kind of prior knowledge that is embedded in the fitting procedure from the outset.

The “suspected resonances” are not the only energy-points that constitute the set  $E_{n\ell}$ . A good fit of the data can only be achieved if, in addition to them, some background energies are included. Usually they are chosen far away (either to the left or to the right) of the energy interval where the measurements were done. The choice of these background energies is made by trial and error.

In contrast to the values of  $E_{n\ell}$ , for the combination coefficients  $\alpha_{n\ell}$  and  $\beta_{n\ell}$  there is no “prior knowledge” and therefore they are treated as the free adjustable parameters. The optimal values

are found by minimizing the following  $\chi^2$  function:

$$\chi^2 = \sum_{i=1}^{N(\text{data})} \left[ \frac{\sigma_{\text{total}}(E_i) - \sigma_{\text{fit}}(E_i)}{\Delta_i} \right]^2. \quad (33)$$

The number of adjustable parameters,  $M$ , depends on the number of terms in Eqs. (31),  $N$ , as well as on  $\ell_{\text{max}}$ ,

$$M = 2(N + 1)(\ell_{\text{max}} + 1). \quad (34)$$

## 6 Numerical example

In order to test the proposed method, we use artificial ‘‘experimental’’ data, i.e. the cross-section data points that were not measured but calculated using a given potential. The uncertainties,  $\Delta_i$ , for such artificial data points are the same for all  $i$ , and can therefore be ignored. The spectrum of the resonant states for this potential is known. After fitting such artificial data, the resonance energies can be found as zeros of the Jost function,  $f_\ell^{(\text{in})}(E)$ , on the unphysical sheet of the Riemann surface. Comparing the results of this search with the known resonance spectrum, we can judge how efficient and accurate the proposed approach is.

The artificial data points were generated with the help of the well-known Noro-Taylor potential with a Coulomb tail (see, for example, Ref. [23]),

$$V(r) = \frac{\hbar^2}{2\mu} \left( 7.5r^2 e^{-r} + \frac{2k\eta}{r} \right), \quad (35)$$

with  $\mu = 1$ ,  $\eta = -1/(2k)$  and  $\hbar c = 1$ . The partial-wave cross-sections for this potential can be calculated using any of the many known methods for solving a two-body scattering problem. One of these methods is based on the direct calculation of the Jost functions (see Refs. [4, 23]), which was used here to find the cross-sections for  $\ell = 0$ ,  $\ell = 1$  and  $\ell_{\text{max}} = 2$ . The total cross-section was then found as the sum of these three partial cross-sections. Some resonances for this potential occur for each  $\ell$ . In particular, the resonances for  $\ell = 0$  were found in Ref. [23].

A relatively small number of 40 data points for the total cross-section were generated in the range  $1.7 < E < 5$ . These ‘‘experimental’’ values were then fitted using Eqs. (12), (13), (14), and the

parametrization (31), with  $N = 3$ . Since  $\ell_{\text{max}} = 2$ , the number of fitting parameters,  $\alpha_{n\ell}$  and  $\beta_{n\ell}$ , defined by Eq. (34), was  $M = 24$ . The values for  $E_{n\ell}$ , apart from the background values, were chosen near known values of  $E_r$ , as is also generally done with  $R$ -matrix fittings. The optimal values for  $\alpha_{n\ell}$  and  $\beta_{n\ell}$  were found by minimizing the  $\chi^2$  function (33) with the help of the minimization routine MINUIT [24]. The chosen  $E_{n\ell}$  and the fitting parameters obtained from the analysis, are given in Table 1. The quality of the fitting can be seen in Fig. 1. The exact and the fitted curves practically coincide within the energy range where the ‘‘data’’ points are available.

The resonance energies (1) were located by finding the zeros of the Jost function,

$$f_\ell^{(\text{in})}(E) = 0, \quad (36)$$

on the unphysical Riemann energy sheet. It should be mentioned that due to the presence of the Coulomb term in the potential, the Riemann surface has spiral topology with an infinite number of sheets [4]. The choice of the correct unphysical sheet is done by taking the appropriate sign in front of the square root  $k = \pm\sqrt{2\mu E}$  and by choosing the principal branch of the logarithmic term in Eq. (10). These choices determine the momentum-dependent and Coulomb-related coefficients in the representation (8). Since  $A_\ell(E)$  and  $B_\ell(E)$  are single-valued, they are the same for all the sheets. Such a separation of all the factors in the Jost function into multivalued (which are always given exactly) and single-valued (which are fitted) parts, is an advantage of the Jost-function method, because the choice of the correct Riemann sheet is always guaranteed.

The exact values of the resonance energies calculated from the potential and those obtained via the fitting are given in Table 2. The values obtained from the fitting are in good agreement

with the exact values. Despite the fact that the first and second resonances for  $\ell = 0$  are far apart from each other and that the second resonance is relatively wide, they are reproduced within the same fitting.

In order to simulate a real-life situation, the fit was done for the total cross-section, i.e. possible deviations of the partial-wave cross-sections from their exact values were not monitored during the fit. It turned out, however, that individual  $\sigma_\ell(E)$  were nicely reproduced as well. This can be seen in Figs. 2-4. Around the resonance energies, the difference of the fitted cross-section curves for  $\sigma_\ell(E)$  from the corresponding exact curves is practically indiscernible. At those energies, where there are no resonances, the fitted cross-sections are not very accurate (see, for example, the discrepancies near  $E = 2$  for  $\sigma_\ell(E)$  with  $\ell = 1$  and  $\ell = 2$ ). This is not something specific to the Jost-function method. Similar inaccuracies also appear in  $R$ -matrix fittings.

Since the proposed approach combines the original Jost-function method (that uses the Taylor series parametrization) with the  $R$ -matrix method, it is logical to compare the new method with both old ones.

For the sake of comparison of the new method with the original Jost-function one, we made an attempt to fit the same data for  $\ell = 0$  within the original method. It turned out that the first two  $S$ -wave resonances could not be found simultaneously from a single fitting. Either the first or the second of these resonances could be recovered when the energy range was split into two sections (around the corresponding  $E_r$ ). Two different fittings with a large number of fitting parameters were required. In contrast, within the modified ( $R$ -matrix type) Jost-function method, the lowest resonances for  $\ell = 0$ ,  $\ell = 1$  and  $\ell = 2$  could be found at the same time from a single fitting of the total cross-section.

For the second comparison, we fitted the same artificial experimental data within the standard  $R$ -matrix approach. In doing this we chose  $B_R = 0$  and tried to use the same values of  $E_{n\ell}$  as in the new method. However, a reasonable fit was only obtained when significantly adjusting the  $E_{n\ell}$  values that correspond to the background. Moreover, we had to choose different values of the channel radius for different  $\ell$ , namely,  $a = 0.53, 1.31, 0.94$  for  $\ell = 0, 1, 2$ , respectively. The optimal parameters of the  $R$ -matrix thus obtained are given in Table 3. The exact and  $R$ -matrix-fitted total-cross-section curves are depicted in Fig. 5. The resonances located as the poles of the corresponding  $S$ -matrix are given in Table 2. As is seen, the accuracy of the obtained resonance parameters is lower as compared to the modified Jost function method. Besides that, the  $R$ -matrix fit requires more effort in finding appropriate values of the arbitrary parameters such as the channel radius and the background  $E_{n\ell}$ .

## 7 Conclusion

Both the Jost-function and the  $R$ -matrix approaches to the analysis of scattering data have their specific advantages and limitations. The main goal of the present study was to show that a hybrid method based on the Jost function analysis with some elements of the  $R$ -matrix method, could be very useful in deducing the resonance parameters from experimental data.

We modified the original Jost-function method in the way the holomorphic parts of the Jost functions are parametrized. Instead of the Taylor series parametrization, we represent the holomorphic parts of the Jost functions similar to the  $R$ -matrix. This modification does not affect the analytic structure of the Jost functions. This allows us to correctly continue the fitted Jost function to complex energies and thus to reliably locate possible resonance spectral points.

In addition to that, far fewer fitting parameters are needed to accurately fit the available data. This is still more than is usually required in the  $R$ -matrix fits, but here there is no dependence on arbitrary values such as the channel radius,  $a$ , and the boundary parameter,  $B_R$ .

Possible generalization of the hybrid method presented here, could be its extension to the analysis of data on the inelastic collisions with several binary channels. In the multi-channel problems the Jost function becomes a matrix and the Riemann surface of the energy  $E$  (on which it is defined) becomes much more complicated, with many branch points and intricate topology [4]. In such a problem, for analytic continuation of the  $S$ -matrix from the real  $E$ -axis

$\ell$	$n$	$E_{nl}$	type	$\alpha_{nl}$	$\beta_{nl}$
0	0			$3.8898 \times 10^5$	$4.9502 \times 10^4$
	1	1.78	resonance	-19.967	30.567
	2	4.0	resonance	$-2.0212 \times 10^5$	$3.0482 \times 10^4$
	3	0	background	$5.3628 \times 10^5$	$9.7332 \times 10^3$
1	0			23.197	-8.3005
	1	3.85	resonance	8.5161	-5.3308
	2	4.75	resonance	180.56	-6.5849
	3	0	background	-185.34	-75.727
2	0			1.3990	1.4942
	1	4.9	resonance	-11.081	0.63462
	2	20.0	background	96.745	-17.167
	3	0	background	14.314	-17.277

Table 1: Chosen  $E_{nl}$  and the corresponding fitting parameters obtained when the artificial total cross-section data-points were fitted using the modified Jost-function method. The data points were generated for the potential (35) within the energy interval  $1.7 < E < 5$ . The “type” indicates if the corresponding parameters are associated with an approximately known resonance energy or if it is related to the background cross-section. According to Eqs. (29), (30) and (31), there are no  $E_{nl}$  for  $n = 0$ . Since this is a model calculation, the units of all the values correspond to  $\hbar c = 1$ .

$\ell$	Exact		Jost function		$R$ -matrix	
	$E_r$	$\Gamma$	$E_r$	$\Gamma$	$E_r$	$\Gamma$
0	1.780524536	$9.5719 \times 10^{-5}$	1.780524652	$9.6022 \times 10^{-5}$	1.780000295	$9.7589 \times 10^{-5}$
	4.101494947	1.157254423	4.100074051	1.126491452	3.984433773	0.733390271
	4.6634611068	5.366401527	—	—	—	—
1	3.8480016342	0.275384458	3.854146542	0.272421209	3.848361301	0.308781678
	4.7500534831	3.505579863	—	—	3.714417102	2.686407215
2	4.9005161451	1.567507025	4.802927949	1.423821138	4.826534238	0.544536450
	5.3006134745	5.884714883	—	—	—	—

Table 2: Exact resonance parameters obtained from the calculations for the potential (35) and the corresponding values found via the modified Jost-function and  $R$ -matrix fit of the artificial data points for  $\sigma_{\text{total}}(E)$  in the energy interval  $1.7 < E < 5$ . The units of all the values correspond to  $\hbar c = 1$ .

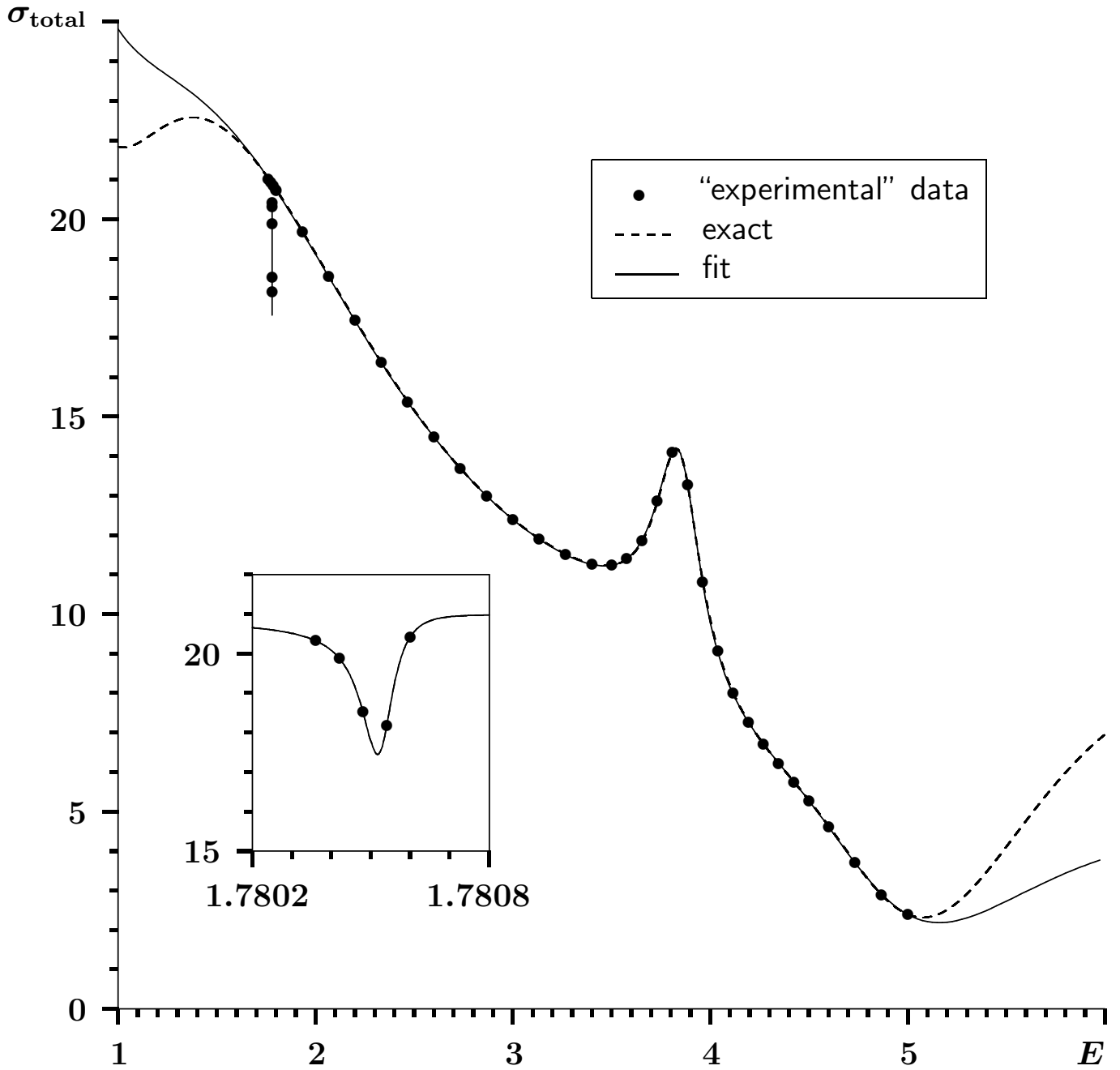


Figure 1: The total cross-section artificial data points (dots) generated using the potential (35). The dashed curve shows the exact cross-section, while the solid curve is what is obtained via the modified Jost-function fit. The cross-section  $\sigma_{\text{total}}(E)$  in the energy interval  $1.7802 \leq E \leq 1.7808$  around the sharp resonance is shown in the insert using a larger energy-scale. The exact and fitted curves are practically indistinguishable in this interval.

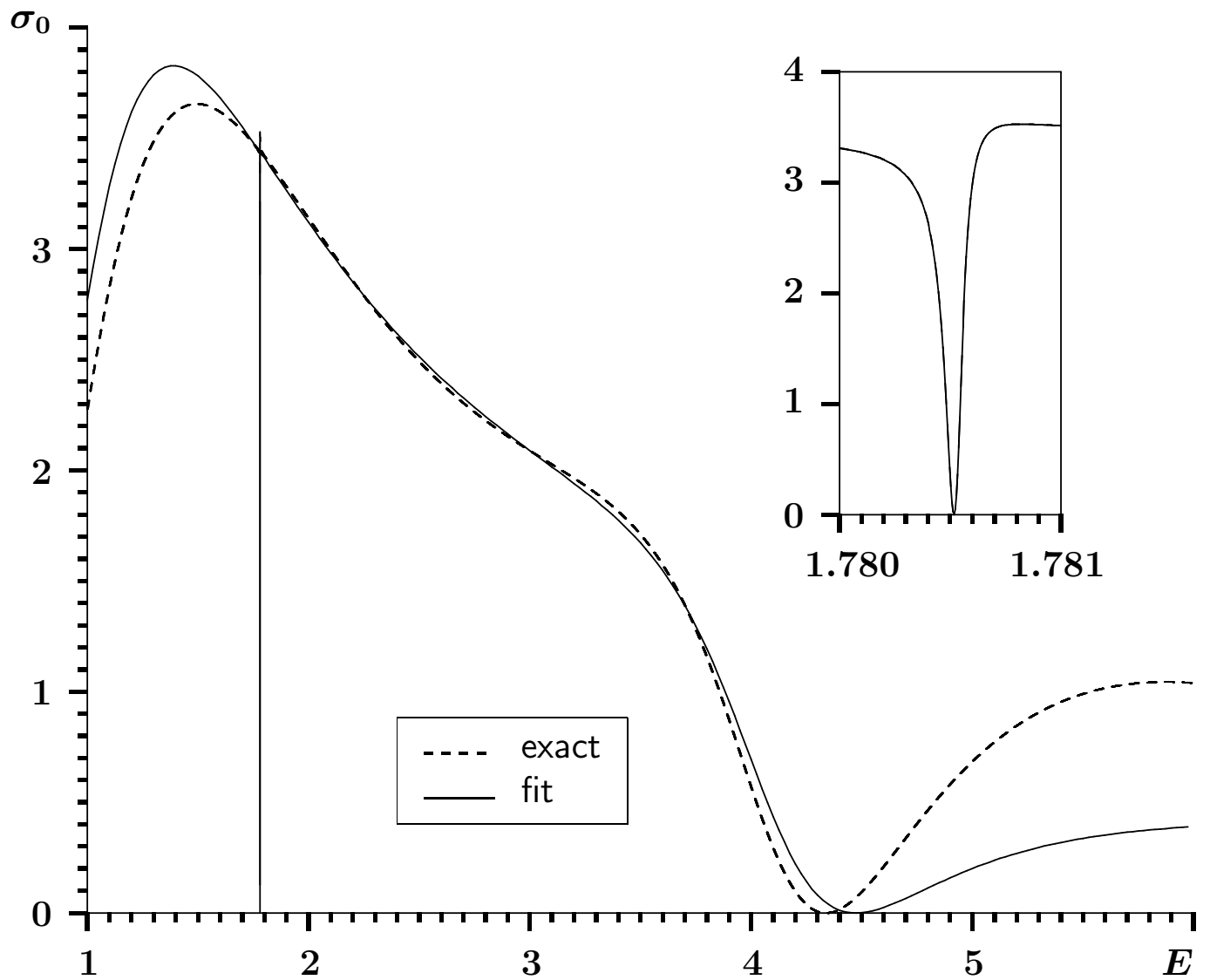


Figure 2: Exact (dashed curve) and fitted (solid curve) partial-wave cross-sections for  $\ell = 0$ . The cross-section  $\sigma_0(E)$  in the energy interval  $1.780 \leq E \leq 1.781$  around the sharp resonance is shown in the insert using a larger energy-scale. The exact and fitted curves are practically indistinguishable in this interval.

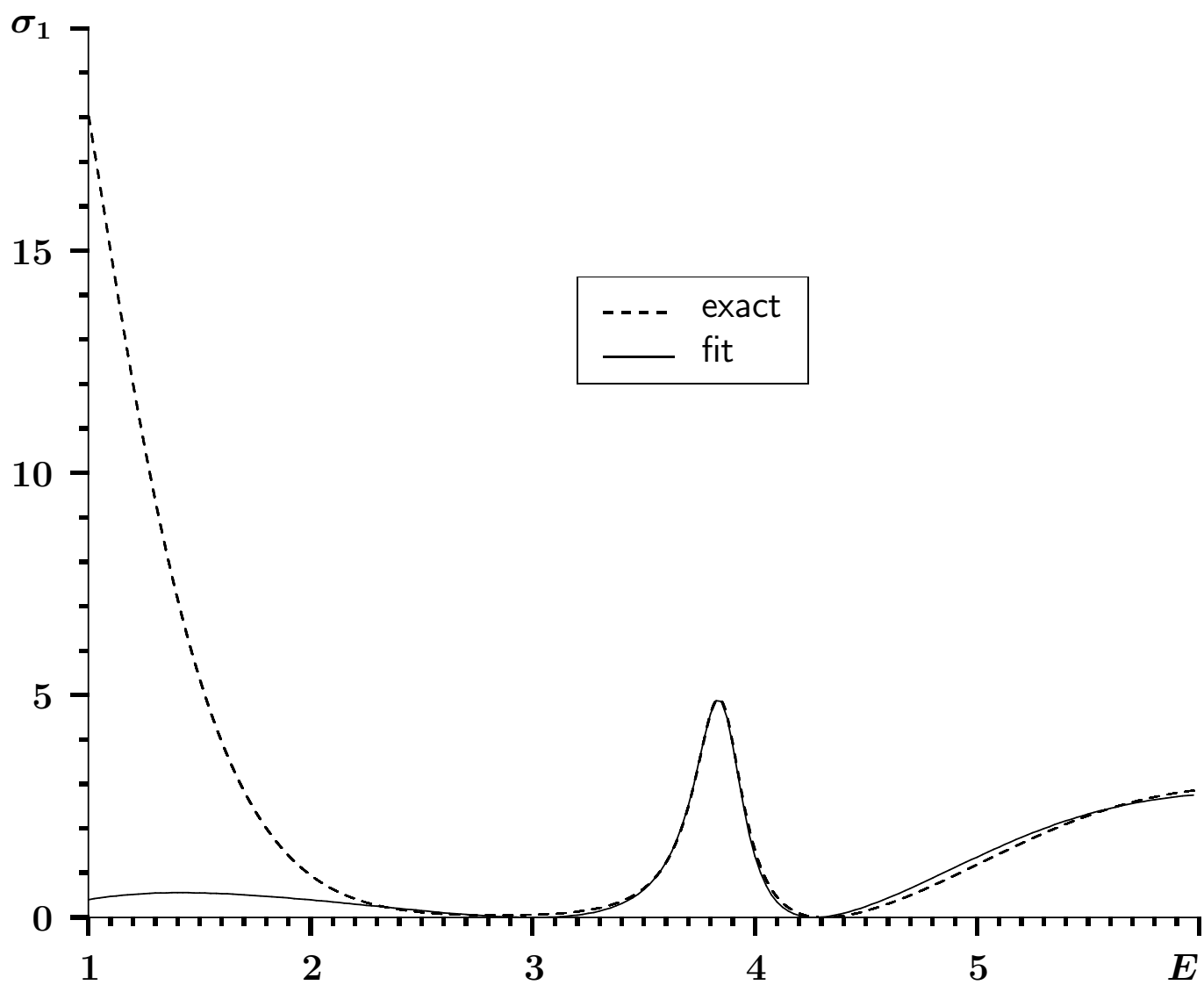


Figure 3: Exact (dashed curve) and fitted (solid curve) partial-wave cross-sections for  $\ell = 1$ .

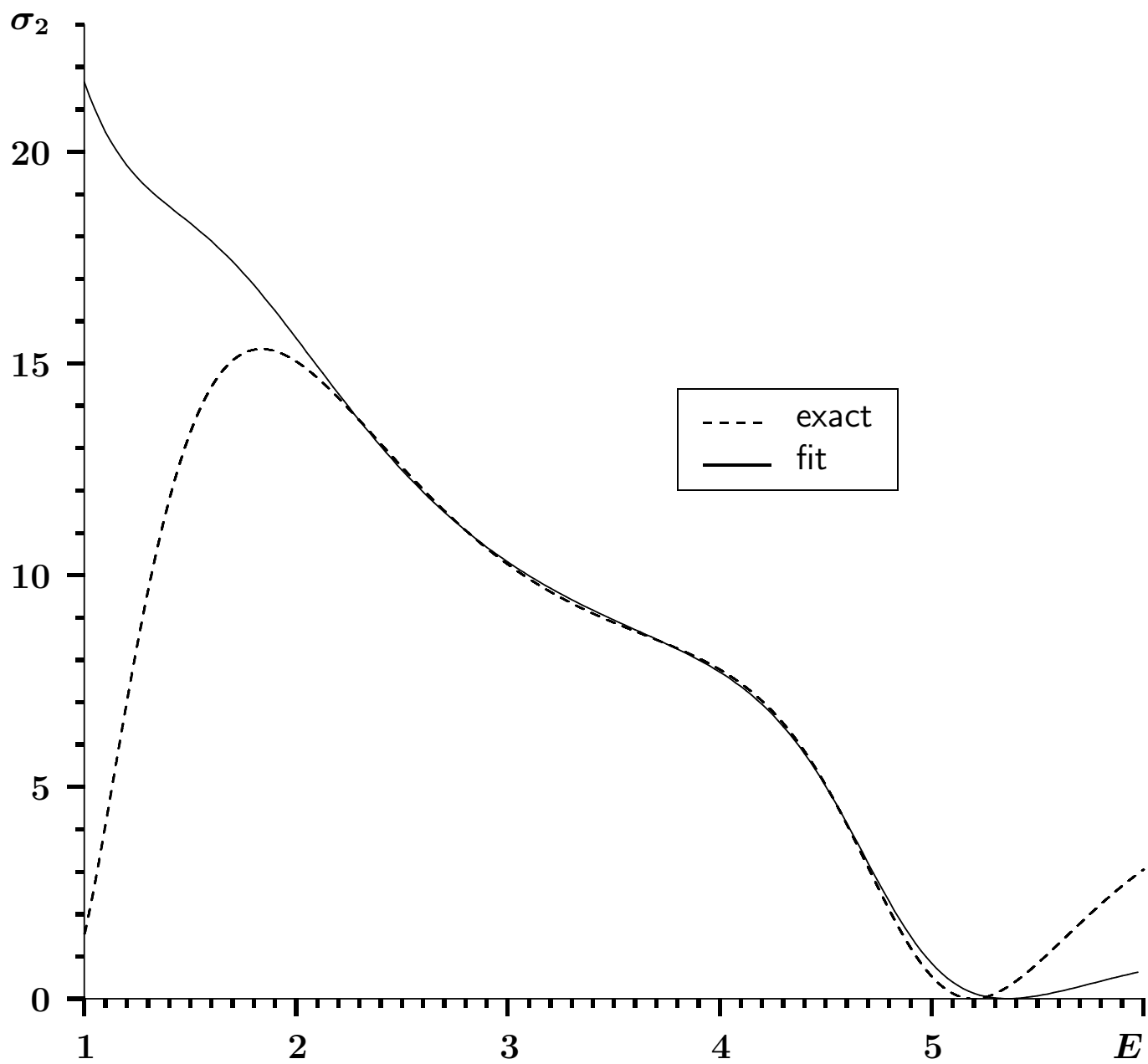


Figure 4: Exact (dashed curve) and fitted (solid curve) partial-wave cross-sections for  $\ell = 2$ .

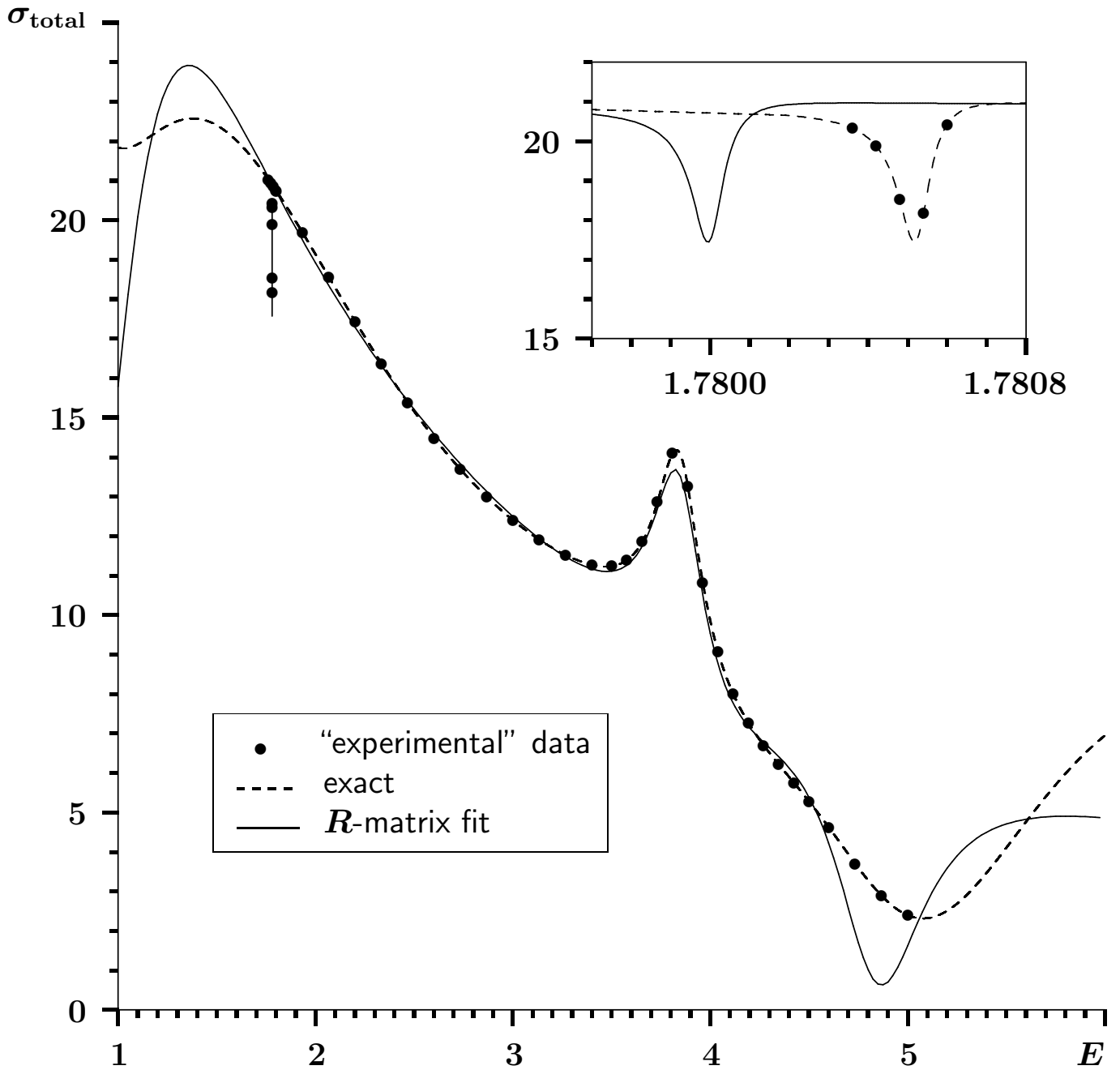


Figure 5: The total cross-section artificial data points (dots) generated using the potential (35). The dashed curve shows the exact cross-section, while the solid curve is what is obtained via the  $R$ -matrix fit. The cross section  $\sigma_{\text{total}}(E)$  in the energy interval  $1.7797 \leq E \leq 1.7808$  around the sharp resonance is shown in the insert using a larger energy-scale.

$\ell$	$n$	$E_{n\ell}$	type	$\gamma_{n\ell}$
0	1	0	background	0.36862
	2	1.78	resonance	$0.59070 \times 10^{-2}$
	3	4.0	resonance	0.44958
	4	20	background	0.88622
1	1	0	background	1.4806
	2	3.85	resonance	0.19240
	3	10	background	$0.10105 \times 10^{-3}$
	4	20	background	3.0343
2	1	0	background	1.2198
	2	4.9	resonance	0.3462
	3	20.0	background	1.5640

Table 3: Chosen  $E_{n\ell}$  and the corresponding fitting parameters  $\gamma_{n\ell}$  obtained when the artificial total cross-section data-points were fitted using the  $R$ -matrix (17) with  $B_R = 0$ . The data points were generated for the potential (35) within the energy interval  $1.7 < E < 5$ . The “type” indicates if the corresponding parameters are associated with an approximately known resonance energy or if it is related to the background cross-section. Since this is a model calculation, the units of all the values correspond to  $\hbar c = 1$ .

it is crucial to have proper analytic structure of the parametrization. This can be guaranteed within the Jost-matrix approach. However, the number of the fitting parameters in the original method (with the Taylor series parametrization) is too large and rapidly grows with the number of channels. This difficulty could be circumvented by incorporating some elements of the  $R$ -matrix theory, as is done here for a single-channel problem.

An example where such a multi-channel hybrid approach could be very useful, is the search for so called “shadow” poles [8,18–22]. These singularities of the  $S$ -matrix are located at complex  $E$  within some unusual domains of the Riemann surface that are different from those where the resonances are. In order to reach these domains, the  $S$ -matrix with proper analytic structure must be used.

## Acknowledgements

This work was funded by the South African National Research Foundation (NRF).

## References

- [1] V.I. Kukulin, V.M. Krasnopol’sky and J. Horáček, *Theory of Resonances: Principles and Applications* (Kluwer Academic Publishers, Dordrecht/Boston/London 1989).
- [2] *Proceeding of the Workshop on the Physics of Excited Nucleons, NSTAR 2005, Tallahassee, October 12–15*, (World Scientific, Singapore, 2006), pp. 1-66.
- [3] J.R. Taylor, *Scattering Theory: The Quantum Theory of Nonrelativistic Collisions* (Dover, New York, 2000).

- [4] S.A. Rakityansky, *Jost Functions in Quantum Mechanics: A Unified Approach to Scattering, Bound, and Resonant State Problems* (Springer, Berlin, 2022).
- [5] S.A. Rakityansky and N. Elander, “Analytic structure of the multichannel Jost matrix for potentials with Coulombic tails”, *J. Math. Phys.* **54**, 122112 (2013).
- [6] P. Vaandrager and S.A. Rakityansky, “Extracting the resonance parameters from experimental data on scattering of charged particles”, *Int. J. Mod. Phys. E* **25** No. 2, 1650014 (2016).
- [7] P. Vaandrager and S.A. Rakityansky, “Residues of the S-matrix for several  $\alpha^{12}\text{C}$  resonances from the Jost function analysis”, *Nucl. Phys. A* **992**, 121627 (2019).
- [8] S.A. Rakityansky and S.N. Ershov, “Jost-matrix analysis of the resonance  ${}^5\text{He}^*(\frac{3}{2}^+)$  near the dt-threshold”, *Int. J. Mod. Phys. E* **28**, No. 8, 1950064 (2019).
- [9] S.A. Rakityansky, S.N. Ershov and T.J. Tshipi, “Resonant states  $0^+$  of the Boron isotope  ${}^8\text{B}$  from the Jost-matrix analysis of the partial cross-sections”, *Int. J. Mod. Phys. E* **28** No. 10, 1950083 (2019).
- [10] P. Vaandrager and S.A. Rakityansky, “Jost-matrix analysis of experimental data on  $d^4\text{He}$  scattering”, *Nucl. Phys. A* **1000**, 121799 (2020).
- [11] E. P. Wigner and L. Eisenbud, “Higher Angular Momenta and Long Range Interaction in Resonance Reactions”, *Phys. Rev.* **72**, 29 (1947).
- [12] P. Descouvemont and D. Baye, “The R-matrix theory”, *Rep. Prog. Phys.* **73**, 036301 (2010).
- [13] R. E. Azuma, E. Uberseder, E. C. Simpson, C. R. Brune, H. Costantini, R. J. de Boer, J. Görres, M. Heil, P. J. LeBlanc, C. Ugalde and M. Wiescher, “AZURE: An R-matrix code for nuclear astrophysics”, *Phys. Rev. C* **81**, 045805 (2010).
- [14] Philip G. Burke, *R-Matrix Theory of Atomic Collisions* (Springer-Verlag, Berlin, Heidelberg 2011).
- [15] M. Abramowitz and A. Stegun (ed.), “*Handbook of Mathematical Functions*”, (NBS, Washington DC, 1964).
- [16] P. Vaandrager, J. Dohet-Eraly and J.-M. Sparenberg, “The Jost function and Siegert pseudostates from R-matrix calculations at complex wavenumbers”, *Eur. J. Phys. A* **60**, 99 (2024).
- [17] J. Humblet, “Analytic Structure and Properties of Coulomb Wave Functions for Real and Complex Energies”, *Annals of Physics* **155**, 461-493 (1984).
- [18] R.E. Brown, N. Jarmie, G.M. Hale “Fusion-energy reaction  ${}^3\text{H}(d,\alpha)n$  at low energies”, *Phys.Rev.*, **C35** (6), 1999-2004 (1987).
- [19] G.M. Hale, Ronald E. Brown, Nelson Jarmie, “Pole Structure of the  $J^\pi = \frac{3}{2}^+$  Resonance in  ${}^5\text{He}$ ”, *Phys.Rev.Lett.*, **59**, 763-766 (1987).
- [20] B.M. Karnakov, V.D. Mur, S.G. Pozdnyakov, V.S. Popov, “Analytic structure of the amplitude of dt scattering near the elastic threshold”, *JETP Lett.* **51** (7), 399-402 (1990).
- [21] I.N. Bogdanova, G.M. Hale, V.E. Markushin, “Analytical structure of the S matrix for the coupled channel problem  $d + t \rightarrow n + \alpha$  and the interpretation of the  $J^\pi = \frac{3}{2}^+$  resonance in  ${}^5\text{He}$ ”, *Phys.Rev.* **C44** (4), 1289-1295 (1991).
- [22] R.M. Id Betan, A.T. Kruppa, T. Vertse, “Shadow poles in coupled-channel problems calculated with the Berggren basis”, *Phys.Rev.* **C97**, 024307 (2018).
- [23] S. A. Sofianos and S. A. Rakityansky, “Exact method for locating potential resonances and Regge trajectories”, *J. Phys. A: Math. Gen.* **30**, 3725–3737 (1997)
- [24] F. James and M. Roos, “Minuit - a system for function minimization and analysis of the parameter errors and correlations”, *Comp. Phys. Comm.* **10**, 343-367 (1975); <http://hep.fi.infn.it/minuit.pdf>